Optimum and Decentralized Detection for Multistatic Airborne Radar

The likelihood ratio test (LRT) for multistatic detection is derived for the case where each sensor platform is a coherent space-time radar. Due to the geometric separation of the platforms, target statistics are modeled as independent from platform to platform but constant over the local data on a single platform. Clutter statistics are also assumed independent from platform to platform but have a local space-time correlation structure typical of monostatic space-time adaptive processing (STAP). Moreover, the target Doppler hypothesis varies from platform to platform due to multiple viewing perspectives.

Previous published work has investigated the detection improvement obtained by multiple input, multiple output (MIMO) radar. This prior work, however, has only considered white noise. When clutter is considered, the diversity benefit of a MIMO or multistatic radar system is strongly dependent on geometry. We investigate the relationship between geometry and diversity gain for multistatic airborne space-time radar and the effects of this relationship on decentralized and centralized detection.

I. INTRODUCTION

Multistatic radars can provide improved performance against stealth targets, protection against attack through the use of stand-off transmitters, and improved performance against electronic countermeasures. Due to these benefits, multistatic radar has been a popular area of research at several times in the last few decades. Currently, the deployment of unmanned air vehicles, the cross-fertilization of multiple-input, multiple-output (MIMO) principles from communication theory, and the increased desire to network sensors together, are again making multistatic radar systems and signal processing an interesting field of study.

Existing work includes results in both optimal multistatic detection [1–2] and decentralized detection [3–11]. In [1], optimum and suboptimum receiver structures are compared for several signal models in the presence of spatially and temporally white Gaussian noise. In [2], detection of signals and noise with various space and time correlation structures is analyzed. In both [1] and [2], each radar platform that contributes to the multistatic system consists of a single spatial channel. Here, each radar platform possesses a multi-channel space-time receiver. Moreover, the target Doppler hypothesis is allowed to vary from platform to platform due to multiple viewing perspectives.

Minimizing the communication bandwidth required to share raw data among sensors is the primary motivation for decentralized methods. The decentralized Bayesian hypothesis test was considered in [3] where it was shown that each sensor implements a local likelihood ratio test (LRT) with local thresholds that are coupled between sensors. In [4] the optimum fusion rule, given the structure of the local tests, was derived. Optimum decentralized Neyman-Pearson detectors have been considered in [5]–[8]. The situation where the local detectors have the constant false-alarm rate (CFAR) property has been considered in [9]–[10], and the impact of fused sensors on area coverage is considered in [11].

In recent years, space-time adaptive processing (STAP) for radar [12–14] has also received significant interest, but the existing work in multistatic detection considers each sensor to consist of a single spatial channel. Therefore, the problem of multistatic STAP, where each sensor platform possesses a coherent space-time radar, has not been fully explored. Each STAP is assumed to reside on a separate airborne platform, which leads to several unique attributes of the current problem compared with the existing literature:

1) Clutter components are assumed to be independent between sensors, and each sensor observes a unique local space-time correlation structure,
2) The amplitude and phase of a target fluctuate independently between sensors but are constant over the space-time data collected at each sensor, and
3) The space-time signature of a target may fall within the clutter ridge for one sensor but not for another.

Multistatic detection is also related to the MIMO radar concept presented in [15]. In [15], MIMO radar was defined as a multistatic system of spatially distributed transmitters and receivers that observe independent target fluctuations. A spatial Swerling II target model [16] was used, that is, the target was modeled as having exponentially distributed radar cross section (RCS) with independent fluctuations in space rather than time. Additive white Gaussian noise (AWGN) was the only interference considered. When clutter is considered, the diversity gain obtained through multiple observations of a fluctuating target depends strongly on geometry. We investigate the relationship between geometry and diversity gain for multistatic airborne radar and the effects of this relationship on decentralized and centralized detection.

Manuscript received July 15, 2005; revised April 21, 2006; released for publication September 6, 2006.

IEEE Log No. T-AES/43/2/903033.

Refereeing of this contribution was handled by M. Rangaswamy.

In the following, we derive the (clairvoyant) LRT for multistatic STAP and use the LRT to assess optimum and decentralized detection performance. Although the clairvoyant case implies that the system is not truly adaptive, for convenience we refer to each radar platform as having a space-time adaptive processor (STAP). In Section II, the assumed signal model is briefly summarized and the LRT is derived. Characteristics such as the mean and variance of the output detection statistic under both hypotheses are also presented since they are used in the signal-to-interference-plus-noise ratio (SINR) metric applied here. In Section III, the decentralized detection rule of [1] is summarized. The LRT and decentralized detection are evaluated via simulated results in Section IV, and conclusions are made in Section V.

II. SIGNAL MODEL AND THE LIKELIHOOD RATIO TEST

In this section, we first summarize the signal model, including assumptions concerning the target and interference characteristics. Then, we derive the LRT for the proposed model and discuss characteristics of the output.

A. Signal Model

Let a multistatic radar system be defined by K different sets of space-time observations of the same volume. In the context of the current work, these sets of observations are statistically independent due to geographical separation of K radar platforms; however, in the general context of MIMO radar they might also represent measurements collected by the same radar platform due to orthogonal transmit waveforms. For example, the data sets may include space-time measurements collected by the same radar over different frequency bands as long as the target and interference observations on the different bands are independent. Let the kth space-time data set be denoted by the vector $\mathbf{z}_k$ for $1 \leq k \leq K$. Each $\mathbf{z}_k$ is formed by stacking the space-time data samples collected by a local multi-antenna array over multiple pulses into a length-N_k column vector where N_k is the number of space-time measurements observed by the kth radar platform. The kth data vector is defined as

$$\begin{aligned} H_0 &: \quad \mathbf{z}_k = \mathbf{n}_k \\ H_1 &: \quad \mathbf{z}_k = a_k \exp(j\phi_k)\mathbf{s}_k + \mathbf{n}_k. \end{aligned} \tag{1}$$

In (1), $\mathbf{n}_k$ is the vector of noise and interference collected by the kth radar, $\mathbf{s}_k$ is the normalized space-time steering vector for the target hypothesis relative to the kth platform, a_k is the unknown amplitude of the target signature, ϕ_k is the unknown phase of the target signature, H_0 is the null hypothesis, and H_1 is the target-present hypothesis. The interference vector $\mathbf{n}_k$ is a zero-mean circularly symmetric, complex Gaussian process characterized by the covariance matrix $\mathbf{M}_k$. Since the target's absolute position and velocity vector map into different relative angles and Doppler shifts for different platforms, each steering vector $\mathbf{s}_k$ is different despite referring to the same target. The target amplitude a_k is Rayleigh distributed with average power $\mathrm{E}[a_k^2] = 2A_k^2$, and ϕ_k is uniformly distributed between zero and 2π. With these assumptions, the vector $a_k \exp(j\phi_k)\mathbf{s}_k$ is a zero-mean complex Gaussian random vector with covariance matrix $\mathbf{S}_k = 2A_k^2\mathbf{s}_k\mathbf{s}_k^{\mathrm{H}}$ where $(\cdot)^{\mathrm{H}}$ denotes the conjugate transpose operator.

The noise vectors, target amplitudes, and target phases are all assumed to be independent from platform to platform. This implies that the geographical separation of the platforms is sufficient to preclude their flight trajectories from overlapping during a coherent processing interval (CPI). Due to the independence assumptions, the joint probability density functions (pdfs) of the data are

$$p(\mathbf{z}_1, \mathbf{z}_2, \ldots, \mathbf{z}_K \mid H_0) = \prod_{k=1}^{K} \frac{1}{\pi^{N_k}|\mathbf{M}_k|} \exp[-\mathbf{z}_k^{\mathrm{H}}\mathbf{M}_k^{-1}\mathbf{z}_k] \tag{2}$$

under the null hypothesis and

$$\begin{aligned} &p(\mathbf{z}_1, \mathbf{z}_2, \ldots, \mathbf{z}_K \mid H_1) \\ &\quad = \prod_{k=1}^{K} \frac{1}{\pi^{N_k}|\mathbf{M}_k + \mathbf{S}_k|} \exp[-\mathbf{z}_k^{\mathrm{H}}(\mathbf{M}_k + \mathbf{S}_k)^{-1}\mathbf{z}_k] \end{aligned} \tag{3}$$

under the target-present hypothesis.

B. Likelihood Ratio Test

The likelihood ratio is defined by

$$\Lambda(\mathbf{z}_1, \ldots, \mathbf{z}_K) = \frac{p(\mathbf{z}_1, \ldots, \mathbf{z}_K \mid H_1)}{p(\mathbf{z}_1, \ldots, \mathbf{z}_K \mid H_0)} = \prod_{k=1}^{K} \frac{p(\mathbf{z}_k \mid H_1)}{p(\mathbf{z}_k \mid H_0)}. \tag{4}$$

Substituting (2) and (3) into (4), taking the logarithm, and simplifying with the matrix inversion lemma yields

$$\zeta = \sum_{k=1}^{K} \frac{r_k^2}{\dfrac{1}{2A_k^2} + \mathbf{s}_k^{\mathrm{H}}\mathbf{M}_k^{-1}\mathbf{s}_k} \tag{5}$$

where $r_k = |\mathbf{s}_k^{\mathrm{H}}\mathbf{M}_k^{-1}\mathbf{z}_k|$. Note that each r_k is the magnitude of a complex Gaussian random variable; therefore, under both hypotheses the test statistic in (5) is a sum of K exponential random variables where the mean of the kth term depends on the target's average power, the target's steering vector, and the interference covariance matrix as observed by the kth radar platform. For any given radar platform,

if the target's expected power is small, then that platform's contribution to the overall test statistic is minimal. If the target's average power is large, then that platform's contribution to the overall test statistic is controlled by the target hypothesis relative to the interference spectrum. Closed-form evaluation of the detection and false alarm probabilities for the detector in (5) requires the cumulative distribution function (cdf) for a weighted sum of exponential variates, which is presented in [17]–[18]. Although the cdf cannot be directly inverted to get the threshold that provides the desired probability of false alarm, the threshold can be easily obtained with a one-dimensional numeric search.

C. Properties of the Test Statistic

Let $C_k = \mathbf{s}_k^{\mathrm{H}}\mathbf{M}_k^{-1}\mathbf{s}_k$ and $D_k = \frac{1}{2}A_k^2 + C_k$. Under the null hypothesis the test statistic is

$$\zeta \mid H_0 = \sum_{k=1}^{K} \frac{\mathbf{s}_k^{\mathrm{H}}\mathbf{M}_k^{-1}\mathbf{n}_k\mathbf{n}_k^{\mathrm{H}}\mathbf{M}_k^{-1}\mathbf{s}_k}{D_k} = \sum_{k=1}^{K} X_{k0}. \tag{6}$$

The mean of each X_{k0} is

$$\mathrm{E}[X_{k0}] = C_k/D_k = \mu_{k0} \tag{7}$$

and the variance of each X_{k0} is

$$\mathrm{Var}[X_{k0}] = \mu_{k0}^2. \tag{8}$$

The mean of the detection statistic under H_0 is

$$\mathrm{E}[\zeta \mid H_0] = \sum_{k=1}^{K} \mu_{k0} \tag{9}$$

and due to the independence assumptions, the variance is

$$\mathrm{Var}[\zeta \mid H_0] = \sum_{k=1}^{K} \mu_{k0}^2. \tag{10}$$

Under the target hypothesis the test statistic is

$$\begin{aligned}\zeta \mid H_1 &= \sum_{i=1}^{K} \frac{\mathbf{s}_k^{\mathrm{H}}\mathbf{M}_k^{-1}(a_k e^{j\phi_k}\mathbf{s}_k + \mathbf{n}_k)(a_k e^{j\phi_k}\mathbf{s}_k + \mathbf{n}_k)^{\mathrm{H}}\mathbf{M}_k^{-1}\mathbf{s}_k}{D_k} \\ &= \sum_{i=1}^{K} \frac{a_k^2 C_k^2 + 2\,\mathrm{Re}\{a_k C_k e^{j\phi_k}\mathbf{n}_k^{\mathrm{H}}\mathbf{M}_k^{-1}\mathbf{s}_k\} + \mathbf{s}_k^{H}\mathbf{M}_k^{-1}\mathbf{n}_k\mathbf{n}_k^{\mathrm{H}}\mathbf{M}_k^{-1}\mathbf{s}_k}{D_k}.\end{aligned} \tag{11}$$

In (11), each term in the summation is again exponentially distributed, but is now made up of three components. The first component is a signal term, the second is a cross term that contains both signal and noise, and the third is the same interference-only output that was present under the null hypothesis. Denote the first, second, and third components as X_{ka}, X_{kb}, and X_{k0}, respectively. Due to the independence of the interference and target parameters, the mean of X_{kb} is zero. The expected value of the first term is

$$\mathrm{E}[X_{ka}] = \frac{C_k^2}{D_k}\mathrm{E}[a_k^2] = \frac{2A_k^2C_k^2}{D_k} = \mu_{ka}. \tag{12}$$

Therefore, the mean of the detection statistic under the target hypothesis is

$$\mathrm{E}[\zeta \mid H_1] = \sum_{k=1}^{K}(\mu_{k0} + \mu_{ka}) = \mathrm{E}[\zeta \mid H_0] + \sum_{k=1}^{K}\mu_{ka} \tag{13}$$

and the variance is

$$\mathrm{Var}[\zeta \mid H_1] = \sum_{k=1}^{K}(\mu_{k0} + \mu_{ka})^2. \tag{14}$$

D. Approximate SINR Metric

In a monostatic STAP scenario, a linear filter $\mathbf{w}$ is applied to the received data, which can be neatly separated into signal and interference components. This leads to a situation where the output signal can also be divided into signal and interference components, and the ratio of output signal power to average output noise power can be computed. In the multistatic case described by (5), however, the cross terms that appear under the target hypothesis (see (11)) make this definition of output SINR difficult to apply because signal and noise cannot be cleanly separated. We would like to evaluate an SINR metric since SINR performance analysis is a hallmark of STAP analysis and provides a good visualization of performance versus target hypothesis. Therefore, in this paper we use the deflection ratio [15, 19] defined as

$$\mathrm{SINR} \triangleq \frac{|\mathrm{E}[\zeta \mid H_1] - \mathrm{E}[\zeta \mid H_0]|^2}{\frac{1}{2}[\mathrm{Var}(\zeta \mid H_1) + \mathrm{Var}(\zeta \mid H_0)]} \tag{15}$$

where expressions for the means and variances have been presented in the previous subsection.

The deflection ratio is not a strict indicator of detection performance unless the test statistic is Gaussian distributed under both hypotheses. Since this is not true for the current situation, we must be careful in how we interpret the SINR metric. One reason that the SINR metric does not strictly indicate performance is that the target amplitude has been allowed to fluctuate, and this fluctuation affects the variance of the target hypothesis as seen from (12) and (14). Hence, as the target's average power is increased, the separation between the means of the two hypotheses increases. However, so does the variance under the target hypothesis, which prevents the output SINR from increasing without bound. We use the SINR metric as a tool for visualizing approximate relative performance between different target hypotheses, not as an absolute performance indicator.

III. DECENTRALIZED DETECTION

The detection statistic in Section II requires significant amounts of data to be shared between radar platforms. In this section, we summarize a decentralized detection scheme designed to limit the required communication bandwidth while operating within a few dB of the LRT. The scheme used is the one proposed in [1]. The approach is to allow each radar to produce its own binary decision, called the local decision. Then, the binary decisions are shared with a centralized processor, which makes a final decision based on a simple Boolean "OR" operation. Other, more sophisticated, decentralized detectors are available; however, our goal here is to characterize how decentralized detection might behave under the unique geometry of airborne multistatic radar rather than to propose or optimize a particular decentralized architecture. For example, the decentralized scheme used here can be optimized through selection of the local false-alarm rates and the fusion order [20], but for simplicity we assume that the local detection threshold at each radar is set such that all radars operate with the same local probability of false alarm, P_F. The results in Section IV show that this approach works well for our application.

Using equal false-alarm rates at each local detector, the exponentially distributed output at each radar under the null hypothesis leads to a threshold at the kth radar of

$$v_k = -\mu_{k0} \ln P_F. \tag{16}$$

For a Boolean OR operation at the central processor, the overall probability of false alarm is approximately [1]

$$P_{FA} \cong K P_F \tag{17}$$

when P_F is small. Likewise, the overall probability of detection is

$$P_D = 1 - \prod_{k=1}^{K} (1 - P_{Dk}) \tag{18}$$

where P_{Dk} is the probability of detection for the kth platform. In the work presented here, we set the local detection threshold using (16), then evaluate P_D using (18) and the known exponentially distributed output of each radar under H_1. In the following section, the detection performance of this simple decentralized scheme is compared with the LRT of Section II under various situations.

IV. RESULTS

In this section, the improvement offered by multistatic configurations is evaluated using output SINR and probability of detection metrics. First, the SINR performance of a one-platform system is compared with that of a three-platform system. Then, multistatic detection performance is analyzed under various configurations of target signal-to-noise radar (SNR) and target hypothesis.

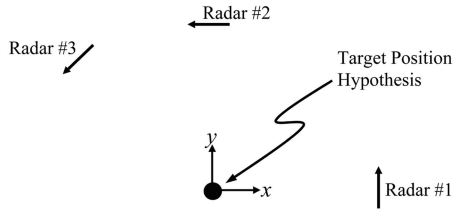

Fig. 1. Multistatic geometry used in SINR and P_D analysis.

The results presented in this section are based on simulation with the following parameters. Up to three radars observe a scene from different aspects as shown in Fig. 1. The direction of travel of each radar is perpendicular to the look direction. The hypothesized target, which is located at the origin of the coordinate system, is in the center of the beam for each radar. Hence, the local azimuth angle to the hypothesized target is zero for each platform. Each radar only receives its own signal.

Each radar has a common set of system parameters such as an operating frequency of 450 MHz, velocity of 100 m/s, pulse repetition frequency (PRF) of 600 Hz, and CPI length of 32 pulses. Each radar uses a twelve-element antenna array with half-wavelength spacing. The interference covariance matrices $\mathbf{M}_k$ are different for each radar with clutter-to-noise ratio (CNR) ranging from 39 to 43 dB. Effects such as antenna misalignment, range-varying clutter power, heterogeneous clutter, and finite sample support are not considered here. We evaluate ideal performance through use of the true interference covariance matrices and accurate target steering vectors. A small amount of internal clutter motion (ICM) has been added via covariance matrix tapers applied to the clutter covariance matrices.

A. SINR Performance

Output SINR is a common metric used in the STAP literature to quantify the ability of a radar system to separate the null and target hypotheses through space-time filtering. The single-platform system observes a null in performance when the velocity of a target along the line-of-sight (LOS) of the platform is small, which causes the target to fall into the clutter notch. The target may be a moving target, but may be moving perpendicular to the radar. A second radar at a different location is able to observe target motion perpendicular to the first radar; therefore, multistatic STAP provides improved performance through geometry as well as through multiple independent observations of a fluctuating target [15]. This effect is clearly seen in the following examples.

Fig. 2 shows an image of SINR performance versus target velocity in the x- and y-directions for the

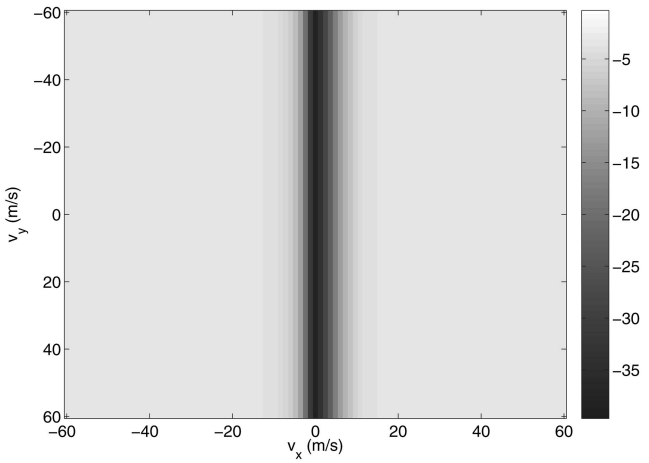

Fig. 2. Output SINR versus target velocity components for a single STAP.

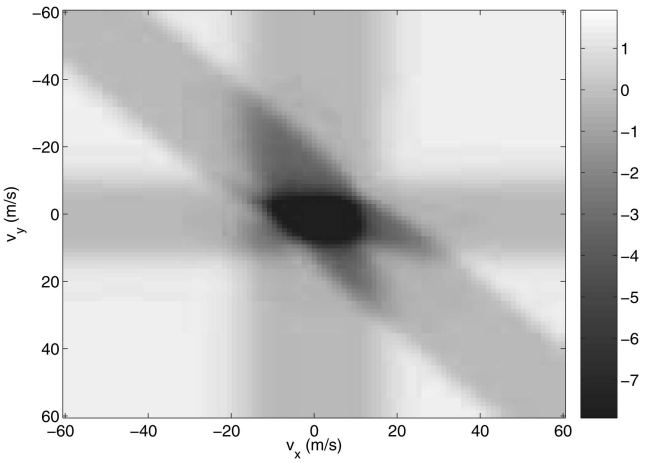

Fig. 3. Output SINR versus target velocity components for three-platform STAP.

first radar. From the geometry of Fig. 1, the first radar can only measure the x-component v_x of the target's velocity. Therefore, when v_x is small, the target falls into the space-time clutter ridge and space-time filtering is ineffective. This reduced performance is seen as a deep notch in SINR performance for small v_x.

When a single radar is used, the direction of motion is just as important as the absolute speed. If multiple radars observe the target from multiple perspectives, however, the target can be detected as long as it is moving in any direction with sufficient speed. This effect is seen in Fig. 3, which shows SINR performance for three radars performing optimum detection. Note the scale change in Fig. 3 that is necessary to clearly show the SINR behavior. If the speed of the target is significant, geometry precludes target motion from being perpendicular to more than one of the radars. Therefore, at least two of the radars are able to separate the target from ground clutter, which leads to an improvement in the best achievable SINR. In Fig. 3, the highest achievable SINR is approximately 1.6 dB compared with -3 dB for Fig. 2. The dips in Fig. 3 occur when the target velocity vector is such that only two of the radars can separate the target from ground clutter; hence, only two independent observations of the target have enough SNR to be useful. The largest improvement is seen around small v_x where the improved geometry of the second and third radars relative to the first radar maximizes the benefit of the additional observations.

For any geometry, the ultimate benefit of multistatic detection is the available diversity gain, which we define here as the reduction in average input SNR needed to achieve the same detection performance as a single-radar system. Since for any one observation, the fluctuating target RCS may be very low, it is valuable to obtain multiple independent observations such that target RCS may be large for one or more of the observations. This is the same principle as diversity combining for communication where a signal may be faded at one measurement but not at another [15, 21]. The benefit of an independent observation, however, depends on the average SNR of that observation; consequently, the geometry of each radar platform controls its diversity gain contribution.

B. Detection Performance

We now consider the detection performance of the optimum and decentralized detectors presented in Sections II and III. The improvement obtained by adding platforms is considered, then the optimum and decentralized detectors are compared for a two-platform system under various assumptions concerning average target RCS and target velocity vector. For all results presented in this section, the overall probability of false alarm has been set to $P_{FA} = 10^{-6}$.

First, we make a comparison between the SINR metric and probability of detection. As mentioned earlier, the deflection ratio does not strictly indicate performance in a quantitative manner unless the test statistic is Gaussian distributed under both hypotheses. In Fig. 4 we show an image of P_D versus target velocity for the same simulation setup used to create Fig. 3. In comparing Fig. 4 with Fig. 3, it is seen that the basic structure of the detection performance is faithfully represented by the deflection ratio; hence, the qualitative intuition obtained in the previous section is valid. Furthermore, for large K the output distributions under both hypotheses will be approximately Gaussian via the central limit theorem, and the deflection ratio will become a more accurate predictor of performance.

Next, the detection performance for one, two, and three platforms is compared for two different target hypotheses. The multistatic configurations for one, two, and three platforms correspond to the same geometry as shown in Fig. 1. The first target

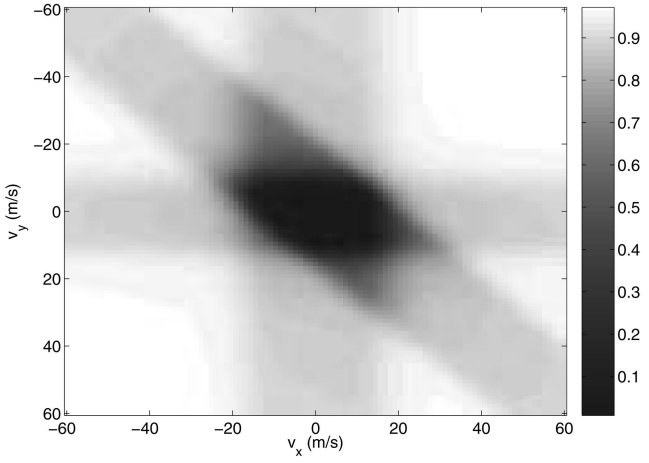

Fig. 4. Image of detection performance for same parameters as in Fig. 3.

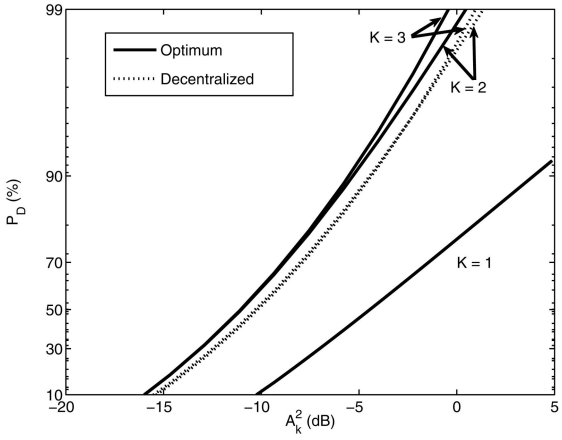

Fig. 5. Detection performance versus average target power for varying number of radar platforms. Target velocity hypothesis is well within third radar's angle-Doppler clutter ridge. $P_{FA} = 10^{-6}$.

hypothesis has $v_x = 10$ m/s and $v_y = 18$ m/s. This corresponds to normalized (to the PRF) Doppler shifts of 0.05, 0.09, and 0.03 for the three radars, respectively. For the given system parameters, the target is partially buried in the angle-Doppler clutter ridge of the first and third platforms, but is mostly separated from clutter in angle-Doppler for the second radar. Detection performance is shown in Fig. 5. For a single platform, the optimum and decentralized detectors are identical. For two and three platforms, the decentralized detector performs worse than the optimum detector; however, the degradation is small. In Fig. 5, the Rayleigh parameter was the same for all platforms, $A_1 = A_2 = A_3 = A_k$.

Detection performance for the second target hypothesis is shown in Fig. 6. In this case, the velocity hypothesis is $v_x = -10$ m/s and $v_y = 18$ m/s, which corresponds to normalized Doppler shifts of -0.05, 0.09, and 0.1 for the three radars, respectively. Since the target falls outside the angle-Doppler clutter ridge for the third radar, the diversity gain provided by the third radar is significantly increased from the

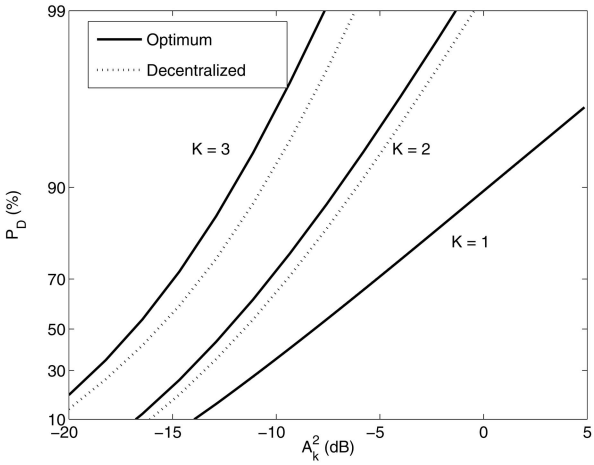

Fig. 6. Detection performance versus average target power for varying number of radar platforms. Target hypothesis is outside angle-Doppler clutter ridge for each radar. $P_{FA} = 10^{-6}$.

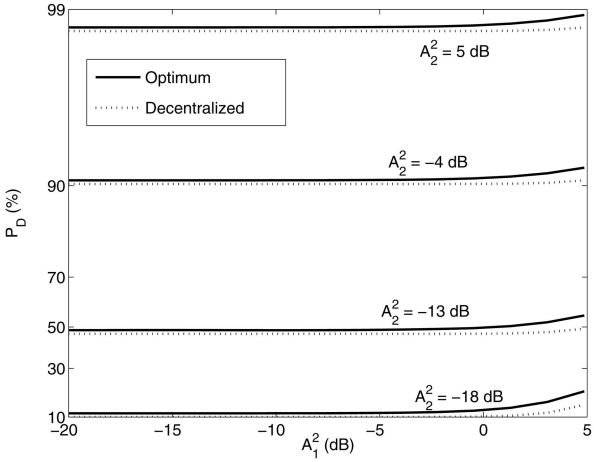

Fig. 7. Detection performance versus average target power for each radar platform. Target hypothesis is within angle-Doppler clutter ridge for first radar. $P_{FA} = 10^{-6}$.

diversity gain seen in Fig. 5. At 90% probability of detection, the diversity gain provided by the second radar in Fig. 5 is approximately 9 dB, but is negligible for the third radar except at high input SNR. In this case, the geometry of the second radar allows diversity benefit while the geometry of the third radar prevents it from making a significant performance contribution. In Fig. 6, the diversity gain at 90% probability of detection is about 7 dB for the second radar, which is reduced from the previous case, but there is 5 dB of additional improvement provided by the third radar.

Next, optimum and decentralized detection are compared for a two-platform system (the first two radars in Fig. 1) under independently varying target RCS. Fig. 7 shows detection performance for $v_x = 3$ m/s and $v_y = 20$ m/s as the Rayleigh parameter A_k is varied independently over both platforms. Probability of detection is plotted versus A_1 and the curves are parameterized by A_2. In Fig. 7, the target

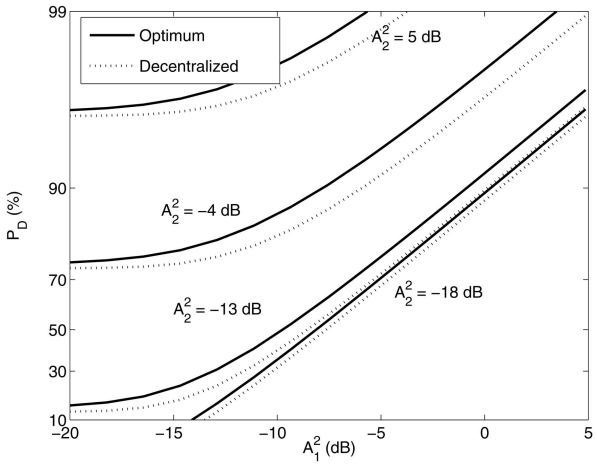

Fig. 8. Detection performance versus average target power. $P_{FA} = 10^{-6}$.

is moving nearly perpendicular to the first radar platform. The effect is that detection performance is nearly independent of A_1 until A_1 becomes large enough that the target is brighter than the surrounding clutter background. The difference in performance between the optimum and decentralized detectors never exceeds a few dB. In contrast, Fig. 8 shows results when the Rayleigh parameters are varied for $v_x = 12$ m/s and $v_y = 16$ m/s. Since the target hypothesis falls outside ground clutter for both radars, performance depends on both A_1 and A_2 at lower input SNR than in Fig. 7.

The above results demonstrate the relationship between geometry and diversity gain achieved through multistatic STAP. The physical geometry clearly controls the contribution of each radar. In Fig. 5, the third radar is in a poor position for detecting the target hypothesis; hence, it's diversity benefit is minimal. The same behavior is also seen for the first radar in Fig. 7. In Figs. 6 and 8, however, large improvements are observed because the target hypothesis is outside the clutter ridge of the additional radar platforms.

The results also show that decentralized detection techniques should perform well for multistatic STAP. For the few cases shown, as well as for other cases evaluated but not presented here, the decentralized OR detector performs within a few dB of the optimum detector. Furthermore, more sophisticated decentralized techniques and optimizations [20] are available, which should push decentralized performance even closer to optimum.

V. CONCLUSIONS

We have presented the optimum detector for multiple independent sets of space-time data, such as might occur for multiple, widely spaced space-time radars. The resulting LRT can be applied to bistatic configurations or to multiple monostatic data collections as long as the target reflection coefficient, noise statistics, and clutter statistics are independent for each data set. The optimum detector is similar to other optimum multistatic detectors [1] in that the detector is a weighted sum of the local LRT results from each sensor. However, analysis of the detector in terms of common STAP parameters and target hypotheses makes clear that performance improvement is obtained through both geometry and diversity gain. Diversity gain refers to the performance improvement obtained by collecting multiple independent observations of a fluctuating target. Geometry gain is obtained by observing a target hypothesis from multiple perspectives such that the target falls outside the observed clutter ridge for one or more of the observing platforms. The results show that geometry gain is essentially a factor that controls the realizable diversity gain.

NATHAN A. GOODMAN
DON BRUYERE
Dept. of Electrical and Computer Engineering
University of Arizona
1230 E. Speedway Blvd.
Tucson, AZ 85721
E-mail: (Goodman@ece.arizona.edu)

REFERENCES

[1] Conte, E., D'Addio, E., Farina, A., and Longo, M.
Multistatic radar detection: Synthesis and comparison of optimum and suboptimum receivers.
IEE Proceedings, Pt. F, **130**, 6 (Oct. 1983), 484–494.

[2] D'Addio, E., and Farina, A.
Overview of detection theory in multistatic radar.
IEE Proceedings, Pt. F, **133**, 7 (Dec. 1986), 613–623.

[3] Tenney, R. R., and Sandell, N. R.
Detection with distributed sensors.
IEEE Transactions on Aerospace and Electronic Systems, **AES-17**, 4 (July 1981), 501–510.

[4] Chair, Z., and Varshney, P. K.
Optimal data fusion in multiple sensor detection systems.
IEEE Transactions on Aerospace and Electronic Systems, **AES-22**, 1 (Jan. 1986), 98–101.

[5] Srinivasan, R.
Distributed radar detection theory.
IEE Proceedings, Pt. F, **133**, 1 (Feb. 1986), 55–60.

[6] Thomopoulos, S. C. A., Viswanathan, R., and Bougoulias, D. K.
Optimal distributed decision fusion.
IEEE Transactions on Aerospace and Electronic Systems, **25**, 5 (Sept. 1989), 761–765.

[7] Thomopoulos, S. C. A., Viswanathan, R., and Bougoulias, D. C.
Optimal decision fusion in multiple sensor systems.
IEEE Transactions on Aerospace and Electronic Systems, **AES-23**, 5 (Sept. 1987), 644–653.

[8] Blum, R. S.
Necessary conditions for optimum distributed sensor detectors under the Neyman-Pearson criterion.
IEEE Transactions on Information Theory, **42**, 3 (May 1996), 990–994.

[9] Barkat, M., and Varshney, P. K.
Decentralized CFAR signal detection.
IEEE Transactions on Aerospace and Electronic Systems, **25**, 2 (Mar. 1989), 141–149.

[10] Barkat, M., and Varshney, P. K.
Adaptive cell-averaging CFAR detection in distributed sensor networks.
IEEE Transactions on Aerospace and Electronic Systems, **27**, 3 (May 1991), 424–429.

[11] Gini, F., Lombardini, F., and Verrazzani, L.
Coverage area analysis for decentralized detection in Weibull clutter.
IEEE Transactions on Aerospace and Electronic Systems, **35**, 2 (Apr. 1999), 437–444.

[12] Guerci, J. R.
Space-Time Adaptive Processing for Radar.
Boston, MA: Artech House, 2003.

[13] Ward, J.
Space-time adaptive processing for airborne radar.
MIT Lincoln Laboratory, Lexington, MA, Technical Report 1015, Dec.1994.

[14] Melvin, W. L.
A STAP overview.
IEEE AES Systems Magazine, **19**, 1, Pt. 2 (Jan. 2004), 19–35.

[15] Fishler, E. et al.
Spatial diversity in radars—Models and detection performance.
IEEE Transactions on Signal Processing, **54**, 3 (Mar. 2006), 823–838.

[16] Peebles, P. Z.
Radar Principles.
New York: Wiley, 1998.

[17] Ali, M. M., and Obaidullah, M.
Distribution of linear combination of exponential variates.
Communications in Statistics—Theory and Methods, **11**, 13 (1982), 1453–1463.

[18] Johnson, N. L., and Kotz, S.
Continuous Univariate Distributions, vol 1.
Boston: Houghton Mifflin, 1970.

[19] Kay, S. M.
Fundamentals of Statistical Signal Processing, vol. II: Detection Theory.
Upper Saddle River, NJ: Prentice-Hall, 1998.

[20] Gini, F., Lombardini, F., and Varshney, P. K.
On distributed signal detection with multiple local free parameters.
IEEE Transactions on Aerospace and Electronic Systems, **35**, 4 (Oct. 1999), 1457–1466.

[21] Goldsmith, A.
Wireless Communications.
New York: Cambridge University Press, 2005.

Analytic Performance Bounds on Estimates of Scattering Center Parameters

Cramér-Rao bounds (CRBs) on the estimates of the main scattering center parameters, i.e., the position, intensity and geometry type, are presented in analytic forms. The resolution limit for wideband radar and the SNR threshold for the correct identification of the geometry type parameter of scattering centers are further deduced. Though the results are obtained from the CRB matrix for damped exponentials (DE) after many approximations and simplifications, their validity and adaptability for geometric theory of diffraction (GTD) based scattering center model have been verified both numerically and experimentally.

I. INTRODUCTION

Radar targets at high frequencies can be well characterized by a few scattering centers. The response of each scattering center is a resonance in the frequency domain. If we ignore the frequency-dependent character of the scattering centers, i.e., assuming ideal point scattering centers [1–3], the target response can then be mathematically modeled as undamped exponentials (UE). However, most scattering centers are frequency dependent in intensity and this dependency is related to the local geometry of the scatterer as predicted by the geometrical theory of diffraction (GTD) [4]. Both exponential function and power function can be used to describe this dependency. The exponential function makes the pole of the exponentials vary a little bit around the unit circle, and therefore the target response has the form of damped exponentials (DE) mathematically [5, 6]. The estimation problem of DE model, or Prony model as it is also named in radar applications, is thoroughly researched with fruitful results [7–9]. The power function is validated to first order by the GTD coefficients of canonical targets [4]. Consequently, this model is called the GTD model whose explicit formation is firstly proposed by the research group led by L. Potter and R. Moses [10, 11]. The power exponent, or the geometry-type parameter as it is usually named, is independent of aspect and relative polarization, which helps in scattering mechanism analysis and scattering center identification. Though GTD model is more difficult to

Manuscript received July 10, 2005; revised April 21, 2006; released for publication October 3, 2006.

IEEE Log No. T-AES/43/2/903034.

Refereeing of this contribution was handled by V. C. Chen.